Bioresource Technology 457 (2026) 134963

Contents lists available at ScienceDirect

Bioresource Technology

journal homepage: www.elsevier.com/locate/biortech

Anti-solvent precipitation of saturated steam autohydrolyzed wheat straw xylan – Regression model-based intensification for biorefineries

Stanislav Parsin *, Martin Kaltschmitt

Institute of Environmental Technology and Energy Economics, Hamburg University of Technology, Eissendorfer Str. 40, 21073 Hamburg, Germany

HIGHLIGHTS

- Derivation of regression models for the relationships of precipitation parameters.
- High yields of high purity xylan precipitated after saturated steam autohydrolysis.
- Evaluation of process parameters affecting yield and precipitate composition.
- Multi-objective parameter optimization for potential applications in biorefineries.

GRAPHICAL ABSTRACT

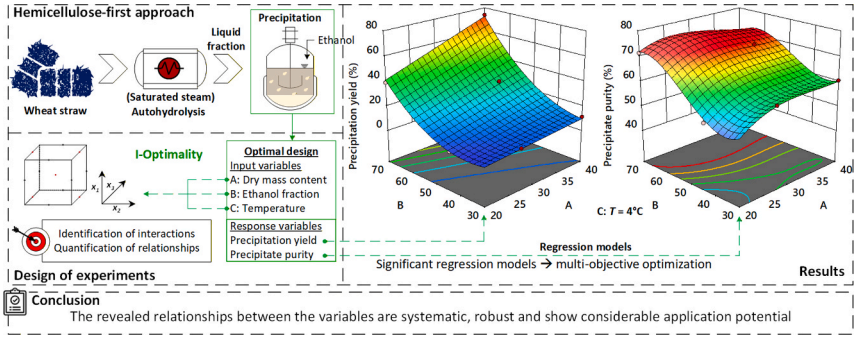

ARTICLE INFO

Keywords:
Ethanol precipitation
Hemicellulose-first
Parameter optimization
Xylooligosaccharides

ABSTRACT

The precipitation of water-soluble carbohydrates using organic solvents offers considerable potential, as separation and purification can be achieved in a single step. Therefore, ethanol precipitation of potential high-value xylan – the main component of wheat straw hemicellulose – is investigated and optimized. Pelletized wheat straw, prepared without chemical or biotechnological auxiliaries, is autohydrolyzed using saturated steam. The pretreatment is designed to effectively solubilize hemicellulose, resulting in a hydrolysate low in impurities that is concentrated and precipitated without further purification. An optimal custom design based on I-optimality is used to systematically investigate the influence of feed concentrate dry mass content (20 to 40 %), ethanol (anti-solvent) fraction (30 to 70 %) and precipitation temperature (4 to 52 °C). Interactions and the effects of selected process parameters on the response parameters "precipitation yield" and "precipitate purity" are qualitatively and quantitatively analyzed using regression models. Highly significant and robust models are derived and validated. The precipitation yield for wheat straw xylan can be well over 70 % (up to 86 %) of the hydrolysate dry mass if a proper hemicellulose-first process design is used. Without intensive downstream processing, wheat straw xylan achieves 82 to 93 % of the carbohydrate content relative to xylan laboratory standards, albeit with differences in composition. The regression models reveal correlations with considerable potential for the valorization of hemicellulose using a relatively simple but optimized hemicellulose-first process. This study provides insights regarding carbohydrate precipitation parameters in a robust, transferable framework, demonstrating their applicability in lignocellulosic biorefineries.

* Corresponding author.
E-mail address: stanislav.parsin@tuhh.de (S. Parsin).

https://doi.org/10.1016/j.biortech.2026.134963
Received 19 January 2026; Received in revised form 2 March 2026; Accepted 23 May 2026
Available online 24 May 2026

1. Introduction

The process of precipitating oligomeric (i.e., degree of polymerization of $\leq$ 10) and polymeric (i.e., degree of polymerization of $>$ 10) carbohydrates from aqueous media through the addition of organic solvents is well-established and widely used within the food industry (Hu and Goff, 2018). This technique is notably relevant for the production of food-grade carbohydrates as well as for non-food-grade carbohydrates, such as those derived from lignocellulose (Peng et al., 2010; Vegas et al., 2004), while separating and purifying polar carbohydrates in parallel (Tang et al., 2020). Thus, this step can enhance the efficiency of biorefinery approaches aiming to produce high-value carbohydrate polymers and oligomers from lignocellulose. Furthermore, such a process step can create valuable synergies within a holistic utilization strategy for lignocellulosic feedstock, especially when organic solvents are concurrently used or produced.

Lignocellulose, as a renewable biogenic resource with the highest global availability related to all organic matter, is widely available as an agricultural byproduct (e.g., wheat straw, rice straw) (Zabed et al., 2016; Zhou et al., 2021). Being often unexplored, straw shows a significant potential for the production of bio-based fuels and chemicals (Mujtaba et al., 2023; Singh et al., 2022). Additionally, high-value byproducts such as biopolymers or biomaterials can be produced from such a feedstock while providing additional incentives for the development of the respective lignocellulose-based biorefineries (Lynd et al., 2022; Santibáñez et al., 2021). In order to utilize lignocellulosic, biomass being *a priori* a limited resource, as completely as possible, a cascade utilization is typically implemented in such biorefineries. Here, various process steps are combined to achieve the highest possible added value based on the three main lignocellulose components cellulose, hemicellulose and lignin. As there is no ideal solution for the effective utilization of all lignocellulose components so far, known concepts often focus on one component and utilize the remaining side streams as byproducts or waste (Renders et al., 2017). In contrast to established cellulose-oriented concepts (i.e., cellulose-first biorefineries), lignin-first concepts are an emerging research topic (Cheng et al., 2024). But also the valorization of pentose-based hemicellulose is still relatively challenging, as, e.g., its use for bioethanol production (by *Saccharomyces cerevisiae* (Qaseem et al., 2021)) is limited and its heterogeneous structure is prone to thermal degradation (Scapini et al., 2021). Organic solvent precipitation coupled with a suitable feedstock fractionation strategy can help overcome such challenges of hemicellulose valorization by providing higher value products such as oligomers and polymers for material use.

Hemicellulose-first approaches aim to maximize the hemicellulose valorization in the initial fractionation step of the overall refinery process (Parsin et al., 2025). A variety of fractionation techniques allowing for such hemicellulose valorization are already known, of which chemical (e.g., alkaline or solvent extraction) and physico-chemical (e.g., autohydrolysis or steam explosion) pretreatment are the most widely used options (Qaseem et al., 2021; Rao et al., 2023). In terms of resource efficient options without chemical auxiliaries, hydrothermal hydrolysis of wheat straw using saturated steam (pure autohydrolysis) can be applied to produce oligomers and polymers based on arabinoxylan, the primary component of wheat straw hemicellulose (Parsin and Kaltschmitt, 2025). Such a concept allows for a relatively energy-efficient fractionation of wheat straw lignocellulose, producing a hemicellulose hydrolysate with low turbidity, indicating low levels of lignin, proteins and other impurities (Parsin and Kaltschmitt, 2023). Consequently, carbohydrates in the hydrolysate can be directly precipitated following, e.g., preliminary filtration and evaporation without prior removal of phenolic components (Parsin et al., 2025). This approach has the advantage of providing solid oligomeric and polymeric hemicellulose, enabling high solids loading for subsequent purification and conversion steps, thus catering to various potential applications (Naidu et al., 2018). Optimizing such a precipitation process can enhance product yield and purity while reducing waste and the consumption of auxiliaries (chemicals, energy and water) aligning with the principles of sustainable circular economy and green chemistry.

For precipitation of carbohydrates from aqueous solutions by adding organic solvents, the yield of the target fraction and the composition of the product are crucial (Hu and Goff, 2018). Therefore, these factors are frequently studied across various laboratory scale studies (Peng et al., 2010; Zasadowski et al., 2014). However, the investigation of such precipitation parameters as well as the respective most important influencing factors has often been realized in parameter ranges being outside the area suitable for a large-scale implementation (e.g., very high solvent loadings, low solids content, low yields) due to techno-economic constraints (Hu and Goff, 2018).

Moreover, previous studies on the precipitation of lignocellulose-derived carbohydrates from a respective solution have tended to be case-specific (Jacquemin et al., 2012; Zasadowski et al., 2014). This is the reason why these investigations provide only fragmented insights into the systematic relationships between influencing factors and precipitation results. Additionally, different experimental conditions might result in partly contradictory conclusions. Xu et al. (Xu et al., 2014), for example, state that precipitation time, temperature and sample concentration are not decisive. However, these are generally considered to be important influencing factors in precipitation (Hu and Goff, 2018). Thus, the transferability of findings and the comparison of methods or parameters are challenging (Han, 2018). A systematic, transferable, and in-depth understanding of parameter interactions during precipitation is therefore an unsolved issue and a clear knowledge gap – especially with regard to the precipitation of hemicellulose carbohydrates extracted from lignocellulosic biomass (e.g., xylan).

Such a systematic investigation of precipitation is not only interesting from a scientific perspective. When considering the assessment of precipitation on a larger scale or for industrial implementation, various influencing parameters (e.g., precipitation temperature, carbohydrate concentration, anti-solvent content) become crucial as they substantially impact the techno-economic success of this process step and thus potentially the entire biorefinery approach. For instance, increasing the concentration of carbohydrates in the precipitation feed via evaporation involves considerable effort, yet subsequently reduces the use of solvents and thereby decreases the effort needed for solvent recovery. Finding an appropriate combination of these interlinked parameters thus results in an optimization challenge for the overall respective biorefinery system. Therefore, the relationships between influencing and evaluation parameters of precipitation, along with their respective interactions, need to be systematically studied and deeply understood.

Against this background, objective of this study is (1) to investigate the relationships and interactions between influencing parameters (dry mass content in the feed solution, anti-solvent fraction and precipitation temperature) and the response parameters (precipitation yield and precipitate purity) during carbohydrate precipitation from hemicellulose hydrolysates. Furthermore, (2) the functional relationships between these influencing parameters are to be captured qualitatively and quantitatively using statistical methods for an adequate representation in mathematical functions. These models are then used (3) to optimize the precipitation process within a hemicellulose-first biorefinery concept. For this purpose, wheat straw is autohydrolyzed using saturated steam focusing on hemicellulose solubilization. The liquid hemicellulose hydrolysate is subsequently concentrated and subjected to precipitation under predefined conditions according to an optimal custom design by adding ethanol as anti-solvent. Regression models are developed based on these lab data. The respective models are evaluated and validated and the results are assessed for their potential to optimize the precipitation process and to identify synergistic interactions for biorefinery applications.

2. Materials and methods

The investigation procedure is shown in Fig. 1 and described in detail below.

2.1. Feed biomass

Pelletized wheat straw (*Triticum austivum*) was used as a feedstock. The pure wheat straw pellets ("Bionesto Stroheinstreu"; article number 8904515) show a diameter of 4 to 6 mm and have been purchased from AGRAVIS Raiffeisen AG (Münster, Germany).

2.2. Experimental procedure

Below, the experimental procedure and specific characteristic values are defined. The investigation of polysaccharide precipitation from produced hydrolysate is described in detail.

2.2.1. Autohydrolysis (steaming)

Wheat straw pellets are prepared and hydrolyzed using only water and thermal energy (Parsin and Kaltschmitt, 2023). First, unwanted organic and inorganic components are removed based on a simple water treatment process. Hence, straw is soaked in water at 60 °C for 20 min and rinsed several times with water at 60 °C. Finally, it is rinsed with deionized water and mechanically dewatered to about 35 to 40 % dry mass. The moist biomass (2 to 3 kg dry mass) is then treated in a 40 L stainless steel fixed bed reactor (custom made) at 180 °C for 35 min with saturated steam. The straw is filled into the preheated high-pressure reactor in a cylindrical cartridge and removed after the reaction time has elapsed and the pressure has been released. According to Equation (3), the severity of the reaction is 3.9 and the liquid-to-solid ratio is 1.5 to 1.9 (Equation (1)). Such autohydrolysis focuses on hemicellulose and has already been studied and described in detail by Parsin and Kaltschmitt (Parsin and Kaltschmitt, 2025). The treated biomass is then extracted with deionized water (20 °C) at a liquid-to-solid ratio of 3 and mechanically dewatered. The liquid phase is vacuum filtered at 5 µm to form the hemicellulose hydrolysate (Fig. 1); nevertheless, the solid residue still contains liquid and solubilized (not extracted) biomass. This is washed off with water and the solid residue is stored at −20 °C.

2.2.2. Precipitation

After steaming (autohydrolysis), the hemicellulose hydrolysate is gently concentrated in a rotary evaporator (Büchi Rotavapor R-100). The pressure is gradually reduced to ca. 150 to 200 mbar (Büchi Vacuum Pump V-100) while maintaining a temperature of around 50 °C (Büchi Heating Bath B-100) until the target dry mass content of 40 % is reached. For experiments requiring a different dry mass content, 4.25 g of concentrate samples are diluted with deionized water according to the design of experiments (section 2.4). At room temperature, no solids settle out at such a high dry mass content, but the concentrate must be mixed very well before aliquoting.

Precipitation experiments were conducted in polyethylene reaction vessels (15 mL and 50 mL). Prior to precipitation, all vessels, as well as the hydrolysate and the absolute ethanol, are preconditioned to the required temperature (section 2.4) in a heating cabinet (Memmert IPP 400). Ethanol is then added and the samples are gently shaken before being maintained at the set temperature for an additional hour to reach equilibrium state. No continuous stirring is required for precipitation.

Following precipitation, the samples are centrifuged at the precipitation temperature for 10 min at 4,760 × *g* (relative centrifugal force) (Hettich Rotixa 50 RS). The precipitate forms a solid pellet separated from the supernatant and subsequently lyophilized (Christ Alpha 1–2 LD). After freeze-drying, the precipitation yield is determined immediately and the samples are stored at room temperature until purity determination (section 2.4).

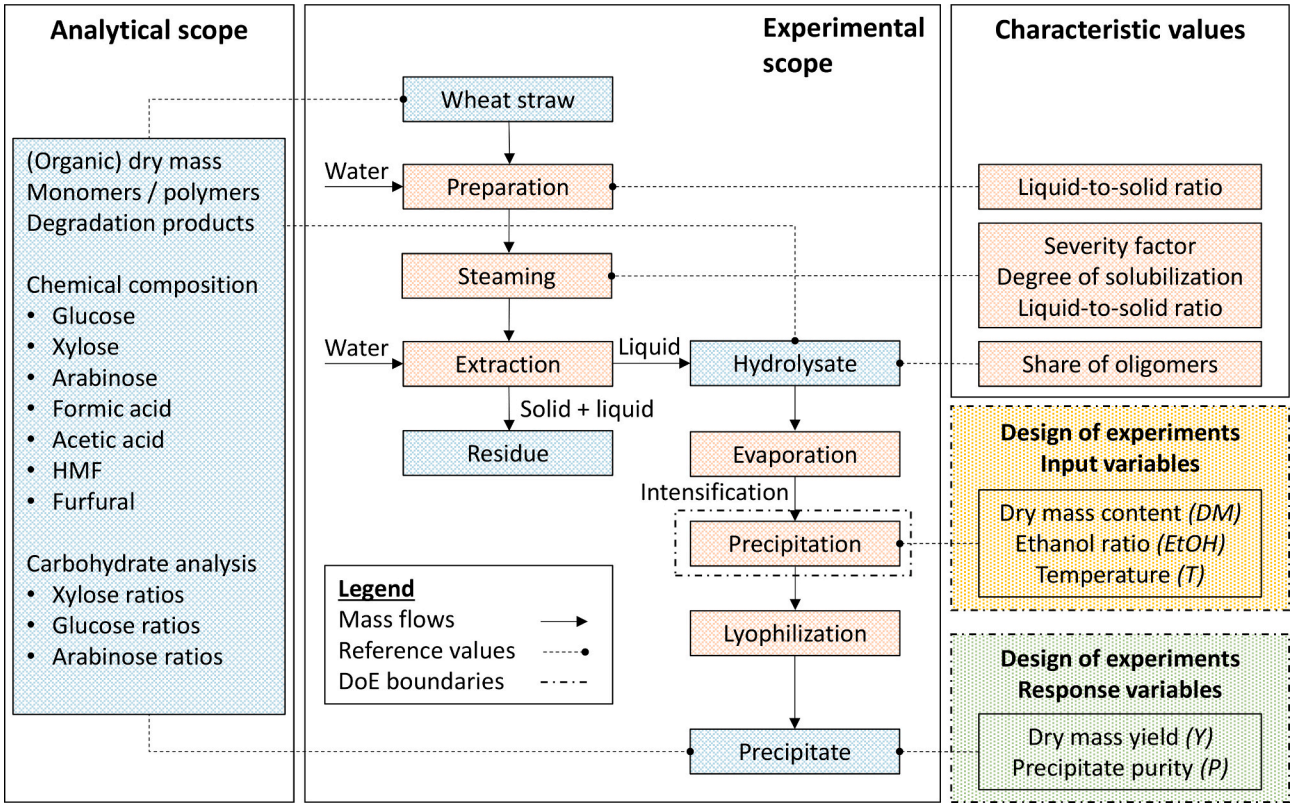

Fig. 1. Scheme of investigation. Experimental process steps are shown in orange and fractions and intermediates in blue. Analytically determined parameters on the left and defined characteristic values as well as design of experiments (DoE) input (yellow box) and output (green box) variables on the right.

2.2.3. Characteristic values

To measure the solvent quantities (e.g., water used for soaking, reaction or extraction), all values are normalized to dry mass. The respective liquid-to-solid ratio (*LSR*) is defined according to Equation (1). To calculate this ratio for a specific process step *j*, the mass of the liquid (*L*) phase (m_j^l) is divided by the dry mass of the solid (*S*) sample (m_j^s) after drying at 105 °C. For water, a density of 1 kg/L is assumed.

$$\frac{L}{S_j} = \frac{m_j^l}{m_j^s} \tag{1}$$

To quantify the intensity of a thermal treatment, a dimensionless severity factor is defined (Brownell and Saddler, 1987; Overend and Chornet, 1987). Using temperature (T in °C) and time (t in min) dependent reaction ordinate R_0 in Equation (2), the severity factor S_0 for nearly isothermal conditions is defined as outlined in Equation (3).

$$\log_{10}(R_0) = \log_{10}\left(t\exp\left(\frac{T(t)-100}{14.75}\right)\right) \tag{2}$$

$$S_0 = \log_{10}(R_0) \tag{3}$$

The autohydrolysis degree of solubilization (*DS*) is calculated using Equation (4), based on the initial solid biomass before (m_0^s) and after (m_1^s) steaming.

$$DS = \frac{m_0^s - m_1^s}{m_0^s}100\% \tag{4}$$

The share of oligomers (i.e., non-monomers) S_i for a component i in the hydrolysate is defined by Equation (5). In this equation, c_i^{mono} represents the measured concentration of the monomeric component i in the sample, while c_i^{total} denotes the total concentration of component i after analytical hydrolysis, including the factor for anhydro correction (*AC*) (section 2.3.3).

$$S_i = \left(1 - \frac{c_i^{mono}}{c_i^{total}}\right)100\% \tag{5}$$

The precipitation yield (*Y*) is determined by the precipitate dry mass ($m_{Pre,DM}$) relative to the initial dry mass of the concentrate ($m_{Conc,DM}$) as described in Equation (6).

$$Y = \frac{m_{Pre,DM}}{m_{Conc,DM}}100\% \tag{6}$$

Since the precipitation of the hydrolysate / concentrate does not only affect carbohydrates as the desired fraction of this process step, the precipitate purity is defined as one key output variable. This precipitate purity (*P*) is determined by the carbohydrate content (m_{CH}) of a precipitate sample (including glucose, xylose and arabinose derived compounds) and expressed as the ratio of these components to the freeze-dried precipitate mass (m_{Pre}) (Equation (7)). Thus, the total concentration of each carbohydrate derived component i after analytical hydrolysis in the water dissolved sample (c_i^{total}) is measured in the sample volume (V_S) and multiplied by the anhydro correction factor (AC_i) (section 2.3.3). The sum of detected carbohydrates is divided by the dissolved precipitate sample dry mass ($m_{S,DM}$).

$$P = \frac{m_{CH}}{m_{Pre}}100\% = \sum_i^n (c_i^{total} AC_i)\frac{V_S}{m_{S,DM}}100\% \tag{7}$$

2.3. Analytical methods

The analytical methods employed, developed, or adapted for component identification and balancing are outlined below. For these procedures, ultrapure water with a maximum conductivity of 0.05 µS cm^{-1} is used. The chemicals utilized in the analytical procedures are of analytical grade.

2.3.1. Compositional analysis

The chemical composition of the feedstock is analyzed using NREL LAP TP-510–42618 (Sluiter et al., 2011) and extractives are analyzed according to NREL LAP TP-510–42619 (Sluiter et al., 2008). For compositional analysis, the dry weight of the acid-insoluble lignin is corrected for ash content. The dry mass content of liquid and solid samples is determined in a drying oven (Memmert U80) at 105 °C. The organic dry mass and the ash content are assessed according to DIN EN ISO 18122 in a muffle furnace (Fisher Scientific M104) at 550 °C.

2.3.2. Quantification of carbohydrates (HPLC)

High-performance anion exchange chromatography with a refractive index detector (HPAEC-RID) (Agilent 1260 Infinity II) is employed to quantify organic low molecular weight compounds (disaccharides, carbohydrate monomers, organic acids, 5-hydroxymethylfurfural and furfural). With the analytical column Agilent Hi-Plex H^+ with a mobile phase of ultrapure water and 5 mM H_2SO_4 relevant monosaccharides (D(+)glucose, D(+)xylose and L(+)arabinose) and disaccharides D-cellobiose and D-xylobiose are determined in a single run. Due to potential peak overlaps from compound coelution in complex samples, xylose results are also confirmed with an Agilent Hi-Plex Pb^{2+} column. For analysis with the Hi-Plex H^+, the flow rate is set to 0.5 mL min^{-1} in isocratic mode, with an injection volume of 10 µL. Both the column and detector are maintained at 55 °C. A seven-point calibration is conducted for all analyzed compounds within the measurement range.

2.3.3. Quantification of oligomeric and polymeric carbohydrates

The carbohydrate content in the liquid phase, released from oligomers or polymers, is indirectly analyzed after hydrolysis to monomers, following the NREL LAP TP-510–42618 guidelines (Sluiter et al., 2011). For the analytical hydrolysis, 10 mL of each liquid sample is filtered (0.45 µm) and then hydrolyzed by adding H_2SO_4 at 121 °C for 60 min (Merck Spectroquant® TR420). Deviating from the NREL LAP TP-510–42618, the amount of H_2SO_4 is reduced to 2 wt-% resulting in a lower furfural concentration. The hydrolyzed samples are subsequently analyzed using HPAEC-RID (section 2.3.2).

2.3.4. Quantification of soluble lignin

The concentration of dissolved lignin in the liquid samples was measured following the NREL LAP TP-510–42618 (Sluiter et al., 2011). Lignin content was assessed using UV spectroscopy at a wavelength of 320 nm, applying a specific absorptivity constant of 30 L $(g\ cm)^{-1}$ on particle-free samples (0.2 µm filtered). Prior to analysis, furfural was entirely eliminated from the samples by means of vacuum evaporation.

2.4. Design of experiments

Response surface methodology is used to investigate the cause-effect relationships of independent (input) variables and dependent (output) variables. The software Design Expert (Version 22, Stat-Ease Inc.) is used for design of experiments (DoE) and the derivation of regression models. The three factors hydrolysate dry mass content (A), the gravimetrical (w/w) ethanol fraction (B) and the precipitation temperature (C) and their investigation range in Table 1 are defined based on available literature data and results from preliminary experiments. An optimal custom design including 30 experimental runs is applied (for further details see supplementary data). The influence of the factors on the response variables and their interactions are examined by coding them ((−1) to (+1), Table 1) and arranging the design points in accordance to I-optimality (Integrated Variance) desirable for optimal predictions by

Table 1
Actual and coded levels of the investigated parameters (factors) used for optimal experimental design.

Factors	Unit	Symbol	Type	Actual values of coded levels	
				−1 (minimum)	+1 (maximum)
Dry mass content (*DM*)	%	A	continuous	20	40
Ethanol fraction (*EtOH*)	%	B	continuous	30	70
Precipitation temperature (*T*)	°C	C	discrete	4	52

response surface methodology (Goos et al., 2016). The design points of the continuous factors are defined by the coordinate exchange algorithm in order to fit the optimality criteria (Harman et al., 2020). For the precipitation temperature, discrete distribution of the design points is applied (i.e., set values of 4, 16, 32, 40 and 52 °C) due to technical restrictions. The precipitation parameters finally implemented experimentally are specified in Table 3.

The following response variables (output parameters) are defined and systematically evaluated.

- The precipitation yield (*Y*) in relation to the total dry mass contained in the hydrolysate before precipitation (Equation (6)).
- The purity (*P*) of the precipitate (Equation (7)).

Based on the measured empirical values, mathematical models are developed for the relationship between the investigated factors (A, B, C) and the response variables. The correlation between a response variable (y) and the coded factors (x_i and x_j) is described by Equation (8). Where c_0 is a constant coefficient, c_i is a linear coefficient, c_{ii} is a quadratic coefficient and c_{ij} is an interaction coefficient. Thus, the correlations are described here using a second-order polynomial function. Corresponding terms can be added for a third-order polynomial if necessary. Model error causing deviation of measured values from predicted values due to unobserved factors, random fluctuations and disturbance variables as well as measuring errors are represented by ε (Siebertz et al., 2010).

$$y = c_0 + \sum_{i=1}^{n} c_i x_i + \sum_{i=1}^{n-1} \sum_{j=i+1}^{n} c_{ij} x_i x_j + \sum_{i=1}^{n} c_{ii} x_i^2 \cdots + \varepsilon \quad (8)$$

In order to evaluate the quality of the statistical correlation between input and output parameters and to quantify the fit, an analysis of variance (ANOVA) and a regression analysis of all models obtained is carried out. The significance of all relevant terms of the descriptive model is tested using the *F*-values with typically required *p*-values below 0.05. The *F*-values, the *p*-values, and the *Lack of Fit* (i.e., remaining variance between the descriptive model and measured values) of the overall models are determined.

In addition, the coefficient of determination (R^2), the adjusted coefficient of determination (*adj.* R^2), the predicted coefficient of determination (*pred.* R^2), and the adequate precision (i.e., signal to noise ratio) are specified for each model.

3. Results and discussion

In the following, the experimental data serving as the basis for the regression models are first presented. Subsequently, the model fit and the relationships between input and output parameters are discussed. Thereafter, model validation and parameter optimization are addressed, followed by a discussion of applications in the context of biorefineries.

3.1. Experimental data

The average ($n = 3$) dry mass content of the wheat straw pellets used is 88.8 ± 0.1 $\%_{FM}$, of which organic dry mass accounts for 93.4 ± 0.1 $\%_{DM}$ and inorganics for 6.6 ± 0.1 $\%_{DM}$. According to the compositional analysis in section 2.3.1 ($n = 3$), this wheat straw consists of 33.1 ± 0.6 $\%_{DM}$ glucan, 26.4 ± 0.4 % arabinoxylan, 20.5 ± 0.4 $\%_{DM}$ lignin and 20.0 ± 0.9 $\%_{DM}$ other compounds.

The hemicellulose hydrolysate produced by saturated steam autohydrolysis (section 2.2.1) has a dry mass content of 3.4 ± 0.2 %. Its carbohydrate composition is presented in detail in Table 2 for the hydrolysate (i.e., after autohydrolysis according to section 2.2.1) and for the concentrate (i.e., post-vacuum evaporation according to section 2.2.2). The concentrations of free components in a native sample (as received) and after complete hydrolysis of carbohydrates with sulfuric acid according to section 2.3.3 (total) are given. Additionally, the share of oligomers (*S*) (i.e., the share of the respective component released from non-monomers by sulfuric acid hydrolysis) is shown in Table 3.

- The degree of solubilization according to Equation (4) is approximately 30 %.
- After vacuum evaporation, the concentrate dry mass content increases to approximately 40 %.
- In the concentrate (considering dilution of 1:10), a (total) xylose concentration of 261.9 ± 0.5 g/L is measured. In the native hydrolysate / concentrate about 85 % of released xylose are present as non-monomers (measured by HPLC; section 2.3.2).
- Depending on pretreatment conditions, carbohydrates represent at least 63 to 76 % of the hydrolysate dry mass (Parsin and Kaltschmitt, 2025, 2023), mainly consisting of water-soluble xylose-based molecules with a broad distribution of molar mass (i.e., xylooligosaccharides and xylan; supplementary data).

The enrichment of dry mass and carbohydrates in the concentrate compared to the hydrolysate is thus 12-fold. Volatile components, such as acetic acid and furfural, are partially lost during evaporation.

Table 3 presents the empirical results according to optimal custom design (section 2.4), which serve as the basis for the derived regression models. In addition to the input parameters (A, B, C) and the response parameters precipitation yield *Y* (Equation (6)) and precipitate purity *P* (Equation (7)), additional parameters are included to further characterize the carbohydrates in the precipitate. Here, Xyl_{Pre} represents the xylose content in the precipitate measured by HPLC, and Xyl_{CH} denotes for the share of xylose in detected carbohydrates. The ratios of the main sugars glucose (*Glu*), xylose (*Xyl*) and arabinose (*Ara*) are also indicated. Furthermore, available laboratory standards, beechwood xylan (BWX) and corn cob xylan (CCX), are included as reference materials to contextualize the results. The analysis and discussion of the findings are presented subsequently.

3.2. Model fit

In design of experiments and response surface methodology, it is crucial to evaluate the model fit, as results regarding relationships and interactions of variables are unreliable without a statistically significant and robust model. Here, an optimal custom design with 30 points is used for the main experiment (Table 3). Such a design is necessary because preliminary trials using a Box-Behnken design with 17 design points have been conducted to define the investigation range in Table 1. These preliminary trials indicate that a Box-Behnken design is insufficient (e.g., low model significance, insufficient *Lack of Fit* and low coefficients of determination) to derive adequate statistical models for the relationships between input and output variables. A high dry mass content (*DM*) of up to 50 % in the concentrate contributed to spontaneous

Table 2
Hemicellulose hydrolysate and concentrate composition. Average ($n = 3$) concentrations and standard deviations (STD) of components in native (as received) and analytically (H_2SO_4) hydrolysed samples (total).

Component	Cellobiose	Glucose	Xylose	Arabinose	Formic acid	Acetic acid	HMF [a]	Furfural
Unit	g/L	g/L	g/L	g/L	g/L	g/L	g/L	g/L
Hydrolysate (native)	0.00	0.00	3.33	1.21	0.56	2.57	0.09	0.63
STD	0.00	0.00	0.04	0.01	0.01	0.04	0.00	0.01
Hydrolysate (total)	0.65	3.55	22.49	1.85	0.60	3.78	0.10	1.27
STD	0.01	0.03	0.07	0.01	0.00	0.01	0.00	0.01
S [b] (%)	100.0	99.9	85.2	34.8	7.3	32.1	15.4	50.5
Concentrate [c] (native)	0.00	0.16	3.96	0.55	0.49	0.68	0.09	0.00
STD	0.00	0.00	0.01	0.02	0.01	0.02	0.00	0.00
Concentrate [c] (total)	0.95	4.12	26.19	2.02	0.52	2.71	0.12	0.81
STD	0.01	0.03	0.05	0.01	0.00	0.01	0.00	0.01
S [b] (%)	100.0	96.2	84.9	72.9	5.6	74.8	24.2	100.0

[a] Hydroxymethylfurfural; [b] Share of oligomers in the hydrolysate and the concentrate according to Equation (5); [c] Diluted for the analysis (1:10) with deionized water.

precipitation of material most likely due to solution super saturation. Under these conditions, experimental yields (Y) of over 85 % are possible, but this behavior leads to disturbances that cannot be captured and represented in significant and reliable regression models (supplementary data).

A good fitting of a model is characterized by high F-values and low p-values (optimally < 0.0001). An adequate *Lack of Fit* is characterized by a p-value between 0.1 and 1.0. The analysis of variance (ANOVA) for the main study using the optimal custom design and maximal *DM* of 40 % in Table 4 indicates a highly significant model (very high model F-values, very low p-values of < 0.0001, high *Lack of Fit* p-value of > 0.1) for both response variables precipitation yield (Y) and precipitate purity (P). Additionally, very high coefficients of determination (maximum 1.0) indicate a good agreement between regression model and empirically measured values. Moreover, the small difference between adjusted R^2 and predicted R^2 (which should not exceed 0.2) confirms adequate model stability and indicates that overfitting has been avoided. For the range of input variables coded according to Table 1, the coded functions (i.e., $Y = f$ (A, B, C) and $P = g$ (A, B, C)) according to Equation (8) can be derived using the coefficients from Table 4 (for results on residual analysis see supplementary data).

The results indicate that reliable and robust regression models can be derived for both response parameters (Y and P). Compared to the precipitation yield (Y), the model for the precipitate purity (P) requires a more complex higher-order polynomial, as multiple cubic terms must be considered to describe the relationships. Within the linear range of the

Table 3
Results of the statistical investigation. The response variables precipitation yield (Y) and precipitate purity (P) are supplemented by further parameters such as the xylose content in the precipitate (Xyl_{Pre}), the xylose content in the detected carbohydrates (Xyl_{CH}), the glucose to xylose (*Glu/Xyl*) and the arabinose to xylose (*Ara/Xyl*) ratio in the precipitate. Notable and high values are highlighted for discussion.

Run	A: *DM*	B: *EtOH*	C: *T*	*Y*	*P*	Xyl_{Pre}	Xyl_{CH}	*Glu/Xyl*	*Ara/Xyl*
	%	%	°C	%	%	%	%	%	%
1	40	30	4	11.2	60.5	41.8	69.1	20.7	6.5
2	30.3	44.4	16	8.8	59.5	36.3	61.0	42.7	5.4
3	23.9	57.8	16	18.6	71.3	40.1	56.2	61.0	2.2
4	26.9	54.2	40	**9.8**	61.4	29.6	48.2	**91.2**	2.8
5	26.9	54.2	40	**7.0**	59.9	27.7	46.3	**99.1**	3.7
6	40	70	52	**48.9**	**70.1**	**46.5**	**66.3**	**33.7**	**2.5**
7	40	30	52	10.8	58.6	40.5	69.1	22.6	5.8
8	20	30	52	3.2	49.3	33.7	68.4	28.0	4.6
9	30.3	44.4	16	8.7	62.5	38.2	61.1	45.2	3.9
10	33	30	40	6.1	56.8	38.7	68.1	24.1	6.7
11	40	58.2	40	33.9	67.8	45.1	66.5	33.1	2.8
12	20	43.4	4	4.1	53.1	31.7	59.6	45.1	6.2
13	20	40	40	2.3	50.2	33.1	66.1	29.7	5.6
14	33	44.8	52	5.5	49.2	31.9	64.7	33.9	5.8
15	35.1	54	4	31.3	70.9	46.6	65.8	33.5	3.5
16	20	61	52	**9.0**	63.3	27.1	42.8	**120.7**	1.2
17	33	44.8	52	6.0	52.5	33.8	64.4	34.3	5.7
18	33	30	40	6.4	56.9	38.7	67.9	24.6	6.6
19	27	30	4	6.1	59.4	41.2	69.3	22.5	6.6
20	40	40.2	16	12.4	61.0	41.0	67.2	27.6	5.7
21	20	30	16	3.3	55.1	36.3	65.8	29.7	6.2
22	26.3	70	52	29.7	70.8	42.0	59.3	51.6	2.0
23	20	70	4	39.2	71.4	45.7	64.0	38.5	1.8
24	23.9	57.8	16	21.4	71.5	41.3	57.7	55.9	2.1
25	26.5	33	28	4.3	55.1	37.2	67.6	26.3	6.0
26	33.2	68.8	40	44.1	70.5	45.9	65.1	36.8	2.2
27	20	70	28	31.3	71.8	43.9	61.1	47.3	1.6
28	39.1	42.3	40	12.3	59.1	39.6	67.0	29.7	5.0
29	34	70	16	**57.3**	**70.9**	**47.8**	**67.5**	**30.1**	**2.9**
30	40	70	4	**73.8**	**69.6**	**48.3**	**69.4**	**25.5**	**3.4**
BWX [a]					77.2	63.7	82.6	3.2	0.0
CCX [b]					87.8	70.1	79.8	13.3	1.8

[a] Beech wood xylan (BWX) purchased from Carl Roth GmbH (Karlsruhe, Germany) (order No. 4414.1); [b] Corn cob xylan (CCX) purchased from Carl Roth GmbH (Karlsruhe, Germany) (order No. 8659.1). The manufacturer's product specification is "≥ 95 % xylooligosaccharides".

Table 4
Regression coefficients and analysis of variance (ANOVA) results. Relevant terms for the derived (coded) regression models for precipitation yield (Y) and precipitate purity (P) according to Equation (8).

Regression coefficients [a]	Y (%)	P (%)
c_0	12.72	62.40
c_A	9.30	1.39
c_B	19.84	15.73
c_C	−5.51	−7.03
c_{AB}	6.35	−2.56
c_{AC}		0.2567
c_{BC}	−5.27	0.6347
c_{AA}		−0.7113
c_{BB}	13.67	3.17
c_{CC}		−1.84
c_{AAC}		3.01
c_{ABB}		−2.32
c_{ACC}		
c_{BBC}		3.57
c_{BCC}		1.45
c_{AAA}		2.54
c_{BBB}		−9.41
ANOVA		
Model F-value	452.75	49.79
Model p-value	< 0.0001	< 0.0001
Lack of Fit (p-value)	0.1396	0.5474
Fit statistics		
Standard deviation	1.90	1.47
Mean	18.90	62.00
Coefficient of variation (%)	10.03	2.38
R^2	0.9916	0.9816
adj. R^2	0.9894	0.9619
pred. R^2	0.9853	0.9134
Adeq. Precision	80.81	21.81

[a] Dry mass content (A), ethanol fraction (w/w) (B), precipitation temperature (C) according to Table 1.

coded design space (Table 1), the regression coefficients (c_A, c_B, c_C) show that the input variables *DM* (c_A) and *EtOH* (c_B) have a monotonic or proportional effect, while T (c_C) exhibits a strictly inverse effect on both response variables. Among these, changes in *EtOH* have the strongest influence on Y and P in the linear range, whereas variations in *DM* have a significantly greater impact on Y than on P. The model F-value and the significant regression coefficients in Table 4 indicate that the variance of the precipitation yield model (Y) is well explained by linear and quadratic relationships. This model involves relatively few regression coefficients and achieves a high F-value of over 450, indicating a robust and significant fit. In comparison, the precipitate purity model (P) includes considerably more regression coefficients but exhibits a substantially lower model F-value. Nevertheless, the purity regression model remains statistically significant and robust indicating more complex relationships of the input and output variables in Table 1.

3.3. Precipitation yield

Fig. 2 illustrates the relationships between the input variables and the precipitation yield (Y) as response surfaces. The empirically measured Y values under the experimental conditions range from 2.3 % to 73.8 %. High Y values consistently correlate with a relatively high ethanol fraction (*EtOH*), high dry mass content in the concentrate (*DM*), and low precipitation temperature (T). However, low T and high *DM* alone are not sufficient for achieving high Y; only when *EtOH* exceeds ca. 50 % (w/w) do Y values rise significantly above 30 %. The models demonstrate that all input variables have a pronounced effect on Y (*EtOH* and *DM* in a monotonic manner, T inversely). According to the regression coefficients in Table 4, the overall influence of *EtOH* is greater in magnitude and, under the examined conditions, can only be partially compensated by the parameters *DM* and T.

The relationships of the actual variables and the precipitation yield (Y) are summarized as a function $Y = f(DM, EtOH, T)$ in Equation (9) for relevant terms. This function can be used for response predictions in the original units for the factors examined.

$$Y = 59.328 - 0.657DM - 3.071EtOH + 0.320T + 0.032DMEtOH - 0.011EtOHT + 0.034EtOH^2 \quad (9)$$

The wide range of resulting values in Fig. 2 indicates a well-founded experimental design and an appropriate parameter range. Some results with low ethanol fractions show low yields of 2 to 4 %. These results confirm that a dry mass content of 40 % does not lead to significant super saturation and precipitation without the addition of ethanol at room temperature.

The anti-solvent precipitation of polar, highly hydrophilic carbohydrates from aqueous media occurs through the reduction of their solubility, which depends on various bonding interactions (Hu and Goff, 2018; Lin et al., 2023). Carbohydrate subunits typically carry polar functional groups (e.g., hydroxyl and carbonyl groups) and primarily interact with water via hydrogen bonding (Lin et al., 2023). Water molecules form hydration shells around polar and charged molecules or ions. The addition of organic solvents like ethanol being fully miscible with water leads to the formation of a more hydrophobic phase, thereby decreasing the dielectric constant of the solvent mixture, the hydrogen bonding capacity and therefore the solubility of polar molecules (Safronov et al., 2019). Under these conditions, solvent polarity decreases, weakening polymer–solvent interactions and making polymer–polymer interactions thermodynamically favored. This behavior of polymers in solutions is described, for example, in the Flory-Huggins theory by the increase in the Gibbs energy of the mixture. Precipitation is induced as soon as a threshold value of Gibbs energy is exceeded (Kishani et al., 2019). This theory explains the relatively strong influence of the ethanol fraction on the precipitation yield in Fig. 2 and Table 4 in comparison to the temperature und the dry mass content. Ethanol fraction directly affects solvent-polysaccharide interactions and acts as the primary thermodynamic driver of precipitation (Safronov et al., 2019). This effect is likely enhanced by adding organic solvents with higher molar mass and more carbon atoms (e.g., propanol and acetone) (Vegas et al., 2005). Thus, anti-solvent precipitation is not selective for carbohydrates alone, but also affects all polar and charged molecules (e.g., proteins, lignin and inorganic substances that can also form complexes (Chen et al., 2024)). Therefore, such impurities and interfering substances in the hydrolysate must be removed effectively beforehand to significantly increase the concentration of the target fraction and the (solid) product purity after precipitation.

Lowering the temperature and increasing the dry mass content further reduce solubility and promote higher precipitation yields (Xu et al., 2014). However, the influence of these parameters is less significant in the study area relative to the ethanol fraction (Table 4). The influence of temperature and dry mass content can be explained by the nucleation-and-growth mechanism (van Delft et al., 1985). Lower temperatures reduce the mobility of molecules (especially water molecules) and mixing in the solution. This can lead to lower xylan solubility due to a reduction in polysaccharide-solvent interactions via hydrogen bonds (Lin et al., 2023). A higher dry mass content presumably promotes the saturation-driven aggregation of solid xylan after addition of ethanol. Higher xylan concentrations in solution lead to a higher nucleation frequency in the solution and faster precipitate particle growth (Thanh et al., 2014).

A disadvantage of the autohydrolysis of hemicellulose that impacts Y is its non-selectivity for a certain fraction in the feedstock (Sun et al., 2022). This leads to the solubilization of other biomass components and results in solubilized hemicellulose xylan having a relatively broad distribution of molar mass in solution (Parsin and Kaltschmitt, 2023). The molar mass of the precipitated xylan molecules (e.g., weight average, number average, viscosity average) has a significant influence on the solubility in aqueous solutions (Swennen et al., 2005). Since polar molecules with a high molar mass also bind a correspondingly large

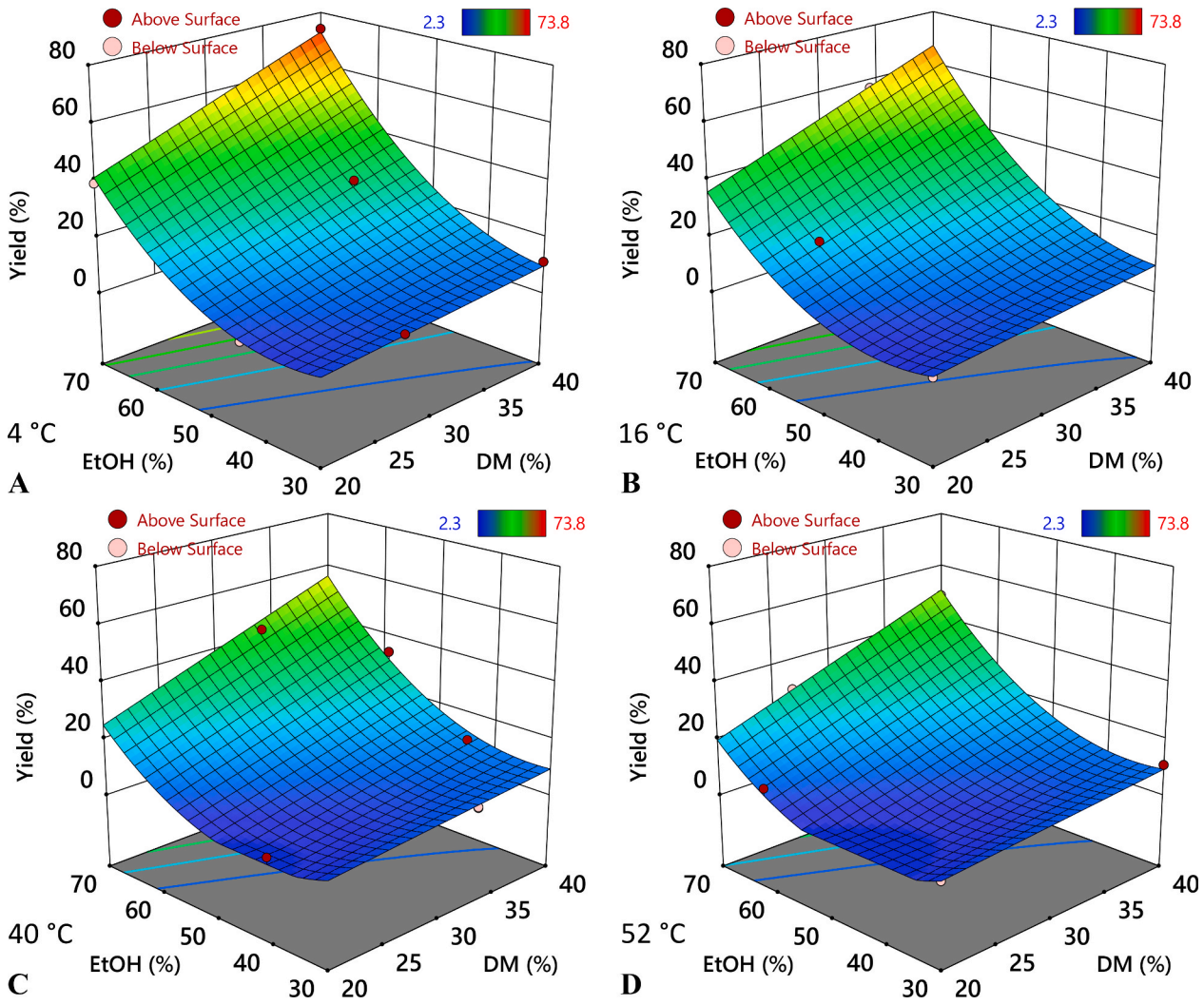

Fig. 2. Response surface results for the precipitation yield according to Equation (6). The precipitation yield is shown as a function of ethanol fraction (*EtOH*) and concentrate dry mass content (*DM*) at different precipitation temperatures; A) 4 °C, B) 16 °C, C) 40 °C, D) 52 °C (28 °C is neglected). The red dots correspond to the measured values.

amount of water molecules via hydrogen bonds, these molecules also increase the Gibbs energy of the mixture the most, in accordance with the Flory-Huggins theory (Safronov et al., 2019); i.e., reduced solubility leads to earlier phase separation with increasing chain length. Consequently, the reduction in the Gibbs energy of the mixture due to their precipitation is also the highest. In this study, the distribution of molar mass of xylan in the hydrolysate and the concentrate is predetermined by autohydrolysis (sections 2.2.1). During precipitation (especially at low precipitation yields), it is to be expected that the high-molecular weight molecules will tend to agglomerate and precipitate first. The higher the precipitation yield, the closer the distribution of molar mass in the precipitate approaches that in the concentrate (supplementary data). This hypothesis is supported by both molecular dynamics models and experimental studies (Lin et al., 2023). Alkaline extraction of hemicellulose leads to the dissolution of polysaccharides with a relatively high molar mass compared to autohydrolysis (Xu et al., 2014). In studies on graded ethanol precipitation, alkaline-extracted hemicellulose shows relatively high precipitation yields at low ethanol fractions (although the absolute yields are often low) (Peng et al., 2010). This is a clear difference from the results for the relatively low-molecular weight xylans after autohydrolysis in Fig. 2. However, without systematic control of the temperature and solids concentration, the total precipitation yields are partly lower despite the high molar mass (e.g., even the high-molecular weight polysaccharides cannot be completely precipitated) (Peng et al., 2009). When evaluating precipitation results, the definition of yield must always be taken into account in all comparisons.

The degree of substitution of the xylan backbone is another important factor that influences solubility and thus precipitation results. Side groups with glucuronic acid, arabinose, and acetyl groups in particular strengthen the xylan-water interactions through a higher average number of hydrogen bonds (Lin et al., 2023). Consequently, it can be assumed that (especially at conditions leading to low precipitation yields) less substituted xylans will precipitate first. However, after autohydrolysis at 180 °C, the degree of substitution of the xylans in the hydrolysate is generally already greatly reduced, which is evident e.g., from the low share of oligomers (*S*) for arabinose and acetate in Table 2 or the arabinose to xylose ratio in Table 3 ((*Ara/Xyl*) varies between 1.2 and 6.7 %). Thus, arabinose and acetate are 65 to 70 % free in the hydrolysate and only about 30 to 35 % bound in non-monomers. The conditions of autohydrolysis significantly affect the degree of substitution of the xylan (e.g., the degree of acetylation). The effects of autohydrolysis conditions on hemicellulose solubilization implemented here have already been studied and show a systematic and predictive

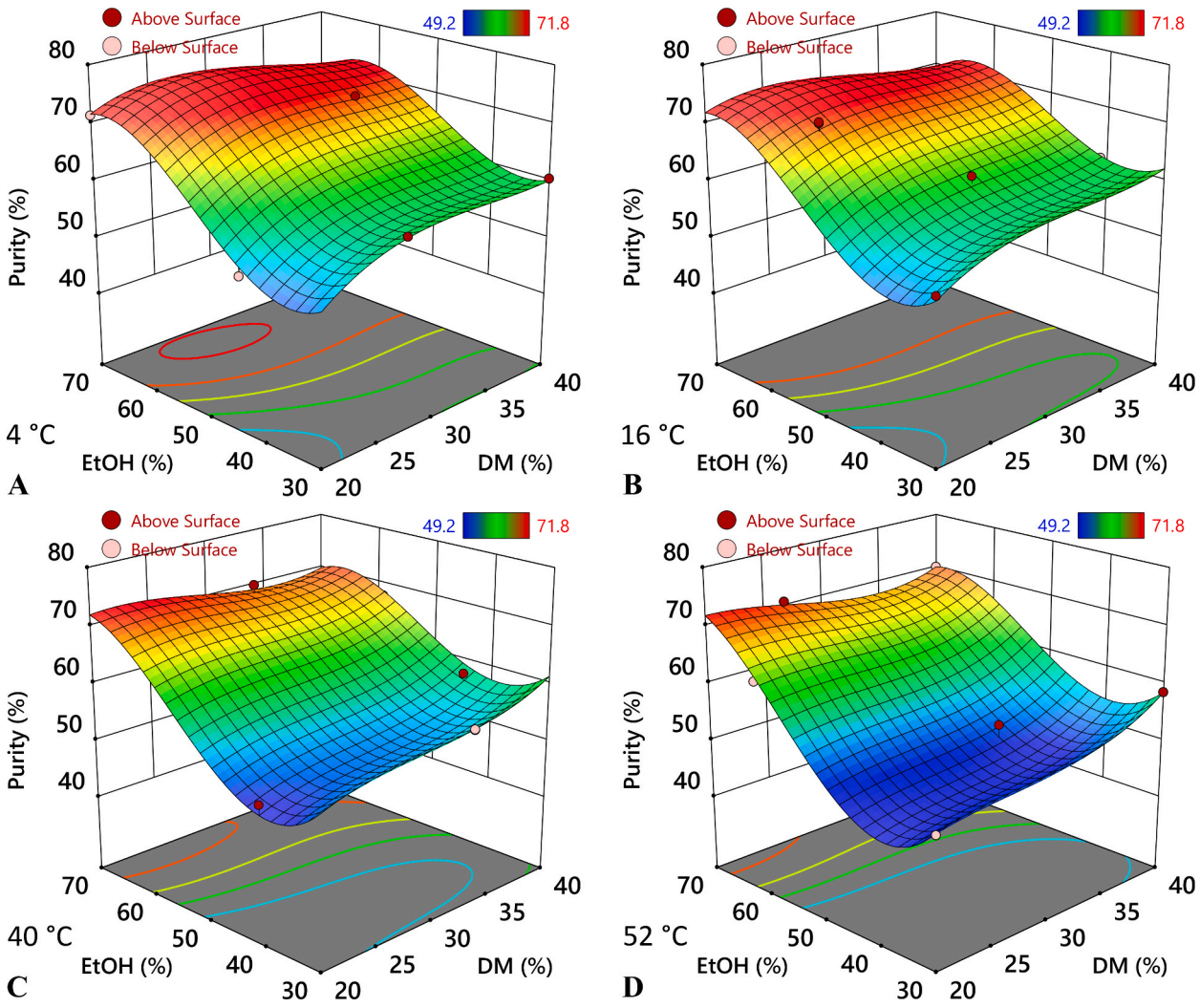

Fig. 3. Response surface results for the precipitate purity according to Equation (7). The precipitate purity is shown as a function of ethanol fraction (*EtOH*) and concentrate dry mass content (*DM*) at different precipitation temperatures; A) 4 °C, B) 16 °C, C) 40 °C, D) 52 °C (28 °C is neglected). The red dots correspond to the empirical (measured) values.

influence on the carbohydrate composition and their substitution degree by arabinose or acetate (Parsin and Kaltschmitt, 2025).

Consequently, not all carbohydrates precipitate simultaneously; instead, they tend to precipitate in stages or sequentially (i.e., starting with those having the lowest solubility). As a result, highly substituted low-molecular weight carbohydrates tend to remain in solution if complete precipitation of carbohydrates is not achieved. These relationships systematically depend on the precipitation conditions, which lead to the variation observed in the response variable *Y*, as shown in Fig. 2 and Table 3.

The response surfaces in Fig. 2 do not indicate that the yield is approaching any limit. Therefore, it is likely possible to further drive *Y* by lowering *T* and increasing *DM* and significantly increase it by raising *EtOH*. Substantially higher yields exceeding 85 % were also empirically confirmed in preliminary trials with 50 % *DM* (supplementary data). However, achieving a quantitative *Y* of 100 % is not desirable, as the concentrate dry mass still contains impurities and precipitated carbohydrates need to be separated from low molecular weight compounds (e.g., sugars, acids, phenols).

3.4. Precipitate purity

Fig. 3 presents the results of the regression models for precipitate purity (*P*) according to Equation (7). The measured values range from 49.2 % to 71.8 % (Table 3) depending on the precipitation parameters (Table 1). These results indicate a significant influence of all three input variables (*DM*, *EtOH*, *T*) on *P*. High *P* values above 65 % are primarily correlated with high *EtOH* levels exceeding 60 %, as also reflected in the high regression coefficients in Table 3. However, under precipitation conditions resulting in very high yields (*Y*) shown in Fig. 2 (i.e., *EtOH* at 70 % and *DM* above 30 %), the purity either stagnates or slightly decreases (Fig. 3). Thus, at $T = 4$ °C, a local optimum for *P* in the investigated range is observed at ca. 65 % *EtOH* and 20 to 30 % *DM*.

The function $P = g(DM, EtOH, T)$ in Equation (10) describes the relationship between the actual input variables and precipitate purity (*P*) for relevant terms. This function can be used for response predictions in the original units for the factors examined.

$$P = 80.765 + 8.702DM - 9.077EtOH + 2.200T + 0.045DMEtOH - 0.074DMT - 0.043EtOHT - 0.271DM^2 + 0.191EtOH^2 - 0.010T^2 + 0.001DM^2T - 0.001DMEtOH^2 + 0.003DM^3 - 0.001EtOH^3 \quad (10)$$

The *P* results in Fig. 3 suggest that initially, a lot of non-xylose-based concentrate components are predominantly co-precipitated, as evidenced by the correlation between low yields (*Y*) and low purity (*P*) in Table 3 (e.g., run No. 8, 12, 13, 14). Subsequently, mainly xylose and glucose containing carbohydrates tend to precipitate. At very high yields

above 60 %, other components (e.g., inorganic substances or complexes of ions and organic molecules (Chen et al., 2024)) alongside carbohydrates are also captured by precipitation resulting in a purity decline (e.g., run No. 29, 30). Another possible explanation is that at high *Y*, low-molecular-weight oligomers are more readily precipitated (Swennen et al., 2005), which, during analytical hydrolysis with H_2SO_4 (section 2.3.3), degrade more extensively than high-molecular-weight ones into monosaccharides and subsequently into volatile degradation products, resulting in greater losses and lower sugar detection according to Equation (7). Such a relationship between input parameters (*DM*, *EtOH*, *T*) and *P* justifies the significant regression coefficients in Table 4, as it can only be represented by a higher-order polynomial function (at least cubic).

The interpretation of precipitate purity results is highly dependent on its definition and the analytical methods used. Since there is no overarching definition for the purity of polysaccharides (Han, 2018), the respective purity must always be transparently described within the context of an investigation. Here, two widely used analytical standards are additionally employed for a classification of the results (Table 3). According to the definition in Equation (7), the measured precipitate purity, e.g., in run No. 27, achieves relative 93 % of beechwood xylan (BWX) and relative 82 % of corncob xylan (CCX) without further purification – but the carbohydrate composition of the precipitate from autohydrolyzed wheat straw differs significantly. The precipitate from wheat straw is more heterogeneous, containing less xylose (low Xyl_{CH}) but more glucose (high *Glu/Xyl*) and arabinose (high *Ara/Xyl*) compared to beechwood xylan and corncob xylan (Table 3).

Notably high *Glu/Xyl* ratios are observed in the precipitates of run No. 4, 5 (duplicate) and 16. These precipitation conditions (DM = 20 to 27 %, $EtOH$ = 54 to 61 %, and T = 40 to 52 °C) do not occur in this combination in any other experiment and result in a relatively low *Y* of 7 to 10 %, low xylose content (Xyl_{Pre} and Xyl_{CH}) and high glucose (*Glu/Xyl*) content. One possible explanation is that under these conditions, high molecular weight carbohydrates (composed of xylose and mainly glucose) are preferentially precipitated, while the lower molecular weight, highly substituted carbohydrates of higher solubility, primarily releasing xylose, do not precipitate as readily. A high degree of polymerization for the glucose-containing carbohydrates was already confirmed in the reference study (Parsin and Kaltschmitt, 2023). A relevant portion of the detected glucose signal may actually originate from glucuronic acid (i.e., a hemicellulose component, not cellulose-based glucan) (Pronyk and Mazza, 2012) which is typically found in wheat straw and may co-elute with glucose under the analytical conditions described in section 2.3.2 (Lai et al., 2016).

The purity definition according to Equation (7) includes only the main sugars (glucose, xylose, and arabinose) and their direct degradation products covered by the analytical procedure described in section 2.3.3. Further sugars (e.g., galactose, mannose) and organic acids (Pronyk and Mazza, 2012) occur in small amounts in wheat straw hemicellulose but are not covered by the purity definition in Equation (7). Besides the identified carbohydrates, other constituents present in the precipitate with a purity (*P*) of over 70 % include the following.

Inorganic components (3 to 12 % w/w; strongly depending on the precipitation yield).
Ethanol-extractable components (5 to 7 % w/w).
Non-ethanol-extractable organic components (not determined).
Free and bound water (4 to 13 % w/w; depending on storage time and composition).

Not all components can be fully accounted for with the analytical methods used (i.e., analytical losses must be considered). For example, the supplier specifies a content of > 95 % xylooligosaccharides for corncob xylan; however, even considering glucose a purity of ca. 88 % is observed here (Table 3). Harsh reaction conditions during analytical hydrolysis can promote the degradation to volatile components like furfural and acetic acid, increasing the losses (Parsin and Kaltschmitt, 2025).

Solubilized lignin occurs in the hydrolysate / concentrate mainly in the form of dissolved phenolic components (Parsin and Kaltschmitt, 2023). The insoluble lignin particles are already separated from the hydrolysate during vacuum filtration after autohydrolysis (section 2.2.1). The soluble phenolic components also precipitate out in part and typically account for 2 to 6 % w/w of the raw precipitate. They presumably form less soluble complexes with inorganic substances and polysaccharides and precipitate out in bound form. This hypothesis is also supported by the fact that a major part of phenolic compounds can be extracted from the precipitate in one step with e.g., ethanol, acetone or propanol. Thus, the soluble phenolic components are usually not covalently bound to the xylans and make up the majority of the ethanol-extractable components in the raw precipitate. However, a small proportion of the phenolic components is not extractable and is presumably covalently bound to the carbohydrates. Such compounds account for less than 0.5 % w/w of the precipitate dry mass.

Inorganic substances can accumulate in the precipitate, as evidenced by their high proportion in the precipitate compared to the hydrolysate dry mass (i.e., 2 to 4 % w/w of the hydrolysate dry mass and 3 to 12 % w/w of the precipitate dry mass) (Parsin and Kaltschmitt, 2025). In samples with a relatively high precipitation yield and high precipitate purity (e.g., runs 6, 29, and 30 in Table 2), inorganics account for between 4 and 5 % w/w of the raw precipitate. Inorganics in the concentrate can form poorly soluble complexes with organic compounds (e.g., phenolic compounds) (Liu et al., 2010). Therefore, raw material preparation and autohydrolysis should aim for a low inorganics content in the hydrolysate dry mass. Previous studies have investigated the release of inorganics during steam-based autohydrolysis and identified a systematic approach that can be used to improve hydrolysate preconditions for precipitation (Parsin and Kaltschmitt, 2025).

The precipitate was deliberately not purified to directly assess the impact of precipitation conditions on *Y* and *P*. A subsequent precipitate extraction with, e.g., (absolute) ethanol would further increase *P* by removing nonpolar and extractable components. These may have previously precipitated as complexes or due to solubility influencing conditions (e.g., concentration, ionic strength, pH value) (Hu and Goff, 2018), but can obviously be extracted from the dry precipitate with organic solvents.

With respect to water content, the precipitate is highly hygroscopic, unlike the standards the samples adsorb water over time. The subsequently measured water content of the samples in Table 3 varied between 4 and 13 % depending most likely on both storage duration and composition. An increased water content likely does not pose a problem for most applications; however, it falsifies the calculated *P* according to Equation (7) downward, as the proportion of carbohydrates (m_{CH}) in the precipitate dry mass (m_{Pre}) decreases.

3.5. Model verification

For model verification, predictions from Fig. 4A were validated through independently conducted experiments. The highest empirically determined precipitate purity so far is 71.8 % (Table 3). However, the regression model suggests potentially higher *P* values at the local optimum (section 3.4). The precipitation temperature (*T*) of 4 °C was kept constant as it allows for good comparability with other polysaccharides (Xu et al., 2014). These conditions are well reproducible in the lab and are often used as reference conditions (Hu and Goff, 2018). For model verification, three random points with high purity (*P*) were selected (Fig. 4B). Model predictions for the corresponding precipitation yield (*Y*) were also verified under specified conditions (Fig. 4A).

Table 5 sums up the regression model verification results for the given precipitation parameters concentrate dry mass (*DM*), ethanol fraction (*EtOH*) and precipitation temperature (*T*).

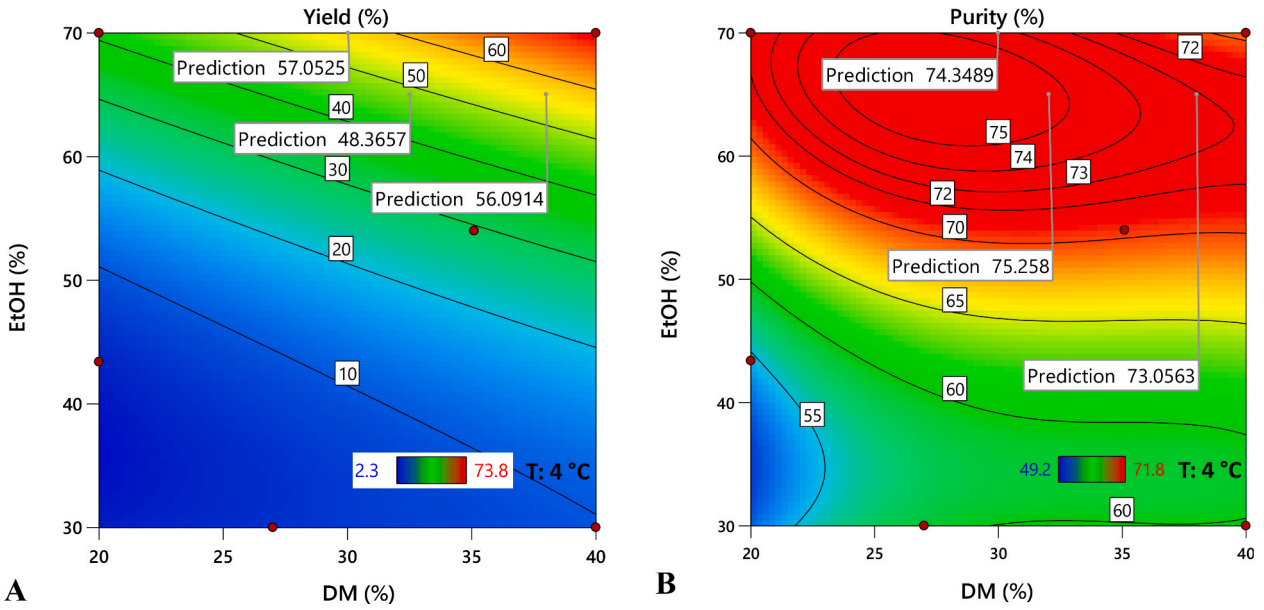

Fig. 4. Contour plots of the precipitation yield (A) and the precipitate purity (B) with indicated values for model verification. The response variables dry mass yield (*Y*) and precipitate purity (*P*) are plotted as a function of the dry mass (*DM*) in the concentrate and the ethanol fraction (*EtOH*) at $T = 4$ °C.

Table 5
Input parameters (*DM*, *EtOH*, *T*) and response values of the model verification. The values for purity and yield predicted by the regression models (Pred. *P* and Pred. *Y*) and those determined independently ($n = 3$) by experiment (Exp. *P* and Exp. *Y*) are tabulated. The relative deviation (Rel. deviation) of the experimental values from the predicted values (basis) is an additional information.

Parameter	*DM*	*EtOH*	*T*	Pred. *Y*	Exp. *Y*	Rel. deviation	Pred. *P*	Exp. *P*	Rel. deviation
Unit	%	%	°C	%	%	%	%	%	%
Verification 1	30	70	4	57.1	52.6 ± 0.3	7.7	74.3	74.2 ± 0.3	0.2
Verification 2	32	65	4	48.4	48.8 ± 2.1	0.8	75.3	73.8 ± 0.4	2.0
Verification 3	38	65	4	56.1	58.5 ± 0.6	4.3	73.1	73.6 ± 0.5	0.8

The small relative deviations for the empirically determined values of *Y* and *P* indicate that the models are robust. This confirms that Equations (9) and (10) can be used for predictions at least within the investigated range.

The verification results can be assessed in the context of statistical evaluation. In Table 4, a higher *pred.* R^2 value is derived for the *Y* model than for the *P* model. This cannot be confirmed by the results in Table 5. The higher deviations for *Y* may be attributed to verification experiments being conducted with different batches of concentrate and ethanol (i.e., deviations in *DM* are possible).

Overall, the results demonstrate that the data support the high model fit stated in section 3.2. Thus, the results can be used, e.g., for precise predictions for optimization purposes (Siebertz et al., 2010). This is evident from the low relative deviations in Table 5 as well as from the independent and separate analytical measurement chains for determining *Y* and *P* (section 2.2.3). Moreover, the verification conditions are at the edge of the investigation range (i.e., $T = 4$ °C and $EtOH \geq 65$ %), where the standard error of the experimental design is typically largest (further results in the supplementary data).

3.6. Parameter optimization

Previous results indicate that the experimental design allows for the deduction of highly significant models for the response variables precipitation yield (*Y*) and precipitate purity (*P*). The investigated approach also enables empirically relatively high *Y* values (section 3.3) along with comparatively high *P* values (section 3.4). The model verification further confirmed the high reliability of the results and identified a local optimum for *P*. Therefore, the regression models can also be used for parameter optimization.

For parameter optimization, a desirability function $D = h$ (*DM*, *EtOH*, *T*) can be applied. This allows for the optimization of either one or both response variables with individually defined weighting. Within such a numerical optimization, only values covered by regression models can be considered, based on their mathematically mapped relationships. The results of such a multi-objective parameter optimization are shown in Fig. 5, where both response variables (*Y* and *P*) are equally weighted. The results for an exemplary single-objective optimization are shown in Table 6.

The desirability function (*D*) in Fig. 5 illustrates how the three input parameters (*DM*, *EtOH*, *T*) can be adjusted to maximize both response variables (*Y* and *P*) equally weighted within the investigated range. The parameters dry mass content (*DM*) and precipitation temperature (*T*) exhibit a linear influence on *Y*, whereas the ethanol fraction (*EtOH*) has an exponential effect. In contrast, only *T* has an approximately linear influence on *P*, while the relationships with *DM* and *EtOH*, as discussed in section 3.4, can only be described by higher-order functions. All three parameters partially exhibit qualitatively opposing effects on the response variables (i.e., for *DM* above 35 % and *EtOH* above 60 %), which will inevitably result in a trade-off. Within the investigated range, the desirability function reaches its maximum at *D* ($DM = 40$ %, $EtOH = 69$ %, $T = 4$ °C), with an optimal value of 94 % for equally weighted optimization.

The results of the individual desirability functions for precipitation yield $D_Y = d_Y(Y)$ and precipitate purity $D_P = d_P(P)$ are listed in Table 6. As already suggested in Fig. 2A, the function value of $d_Y(Y)$ reaches a

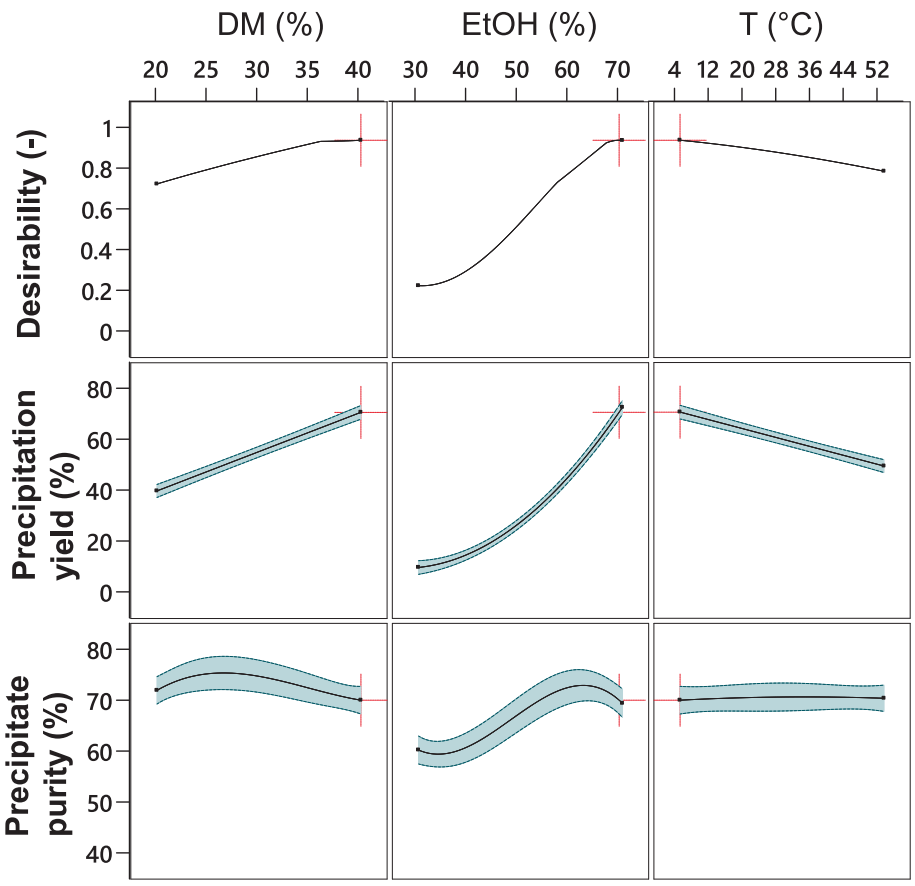

Fig. 5. Multi-objective optimization results. Influence of the actual input variables dry mass content (*DM*), ethanol fraction (*EtOH*) and precipitation temperature (*T*) on the modeled precipitation yield (*Y*) and precipitate purity (*P*) as well as the desirability function (*D*). The blue band represents the 95 % confidence interval, indicating the uncertainty of the model for *Y* and *P* predictions. The desirability function (*D*) was derived under the constraint of maximizing both *Y* and *P* (equally weighted). The cross marks the conditions of numerically optimized desirability, which reaches its maximum functional value of 94 % at D_{max} (DM = 40 %, *EtOH* = 69.3 %, *T* = 4 °C).

Table 6
Single-objective optimization results. Desirability and the (actual) input variables dry mass content (*DM*), ethanol fraction (*EtOH*) and precipitation temperature (*T*) are given for optimized precipitation yield (*Y*) and precipitate purity (*P*). The desirability function was calculated under the constraint of maximizing the respective response variable (*Y* or *P*) according to defined weighting (0 or 100 %).

Weighting (%)		Results (%)		Desirability	*DM*	*EtOH*	*T*
Yield (*Y*)	Purity (*P*)	Yield (*Y*)	Purity (*P*)	(%)	(%)	(%)	(°C)
100	0	72.7	69.4	98.4	40	70	4
0	100	37.4	74.9	100.0	29.9	62.2	7.3

maximum of 98.4 % at D_Y (*DM* = 40 %, *EtOH* = 70 %, *T* = 4 °C). The experimentally determined *Y* of 73.8 % (Table 3) under these conditions is even higher than the model prediction of 72.7 %. In contrast, the maximum value of the purity desirability function d_P (*P*) is achieved at 100 % for D_P (*DM* = 29.9 %, *EtOH* = 62.2 %, *T* = 7.3 °C) due to the interactions discussed in section 3.4.

Fig. 5 illustrates that, in general, a high *DM*, a high *EtOH* and a low *T* are favorable when aiming to maximize both response variables (*Y* and *P*) simultaneously. Capturing the interactions of influencing parameters and precipitation results through multi-objective optimization, particularly after autohydrolysis, can contribute significantly to their comprehension and application.

4. Potential applications

The practical feasibility of a precipitation step must be assessed within the context of the associated raw material utilization strategy. For the most efficient integration of the precipitation step into a biorefinery concept, the precipitation parameters must be evaluated and optimized not in isolation but as part of the process cascade. The investigated biorefinery concept is based on a hemicellulose-first approach with a saturated steam autohydrolysis as the initial lignocellulose fractionation step (Parsin and Kaltschmitt, 2025).

The respective parameter optimization in section 3.6 is performed numerically based on regression models; i.e., it does not account for the necessary process-related efforts. The precipitation conditions derived from numerical optimization may not necessarily be practical for the application within a biorefinery. For instance, cooling the entire hydrolysate to 4 °C immediately after autohydrolysis at 180 °C or evaporation at 50 °C could require significant energy input. This is particularly disadvantageous if the supernatant of the precipitation must then be reheated again for solvent recovery via distillation. Instead, synergies within the process sequence should be leveraged and a custom solution for the optimization problem need to be found as a target-specific parameter combination (Xu et al., 2014); i.e., the study outlined can only provide a transferable basis and methodology for such an approach.

While Fig. 5 illustrates the relationships between input and response parameters through regression models,

Fig. 6 shows the precipitation conditions under which both high precipitation yields (*Y*) and high precipitate purity (*P*) were empirically achieved. The results indicate that high ethanol fractions (*EtOH* over 60

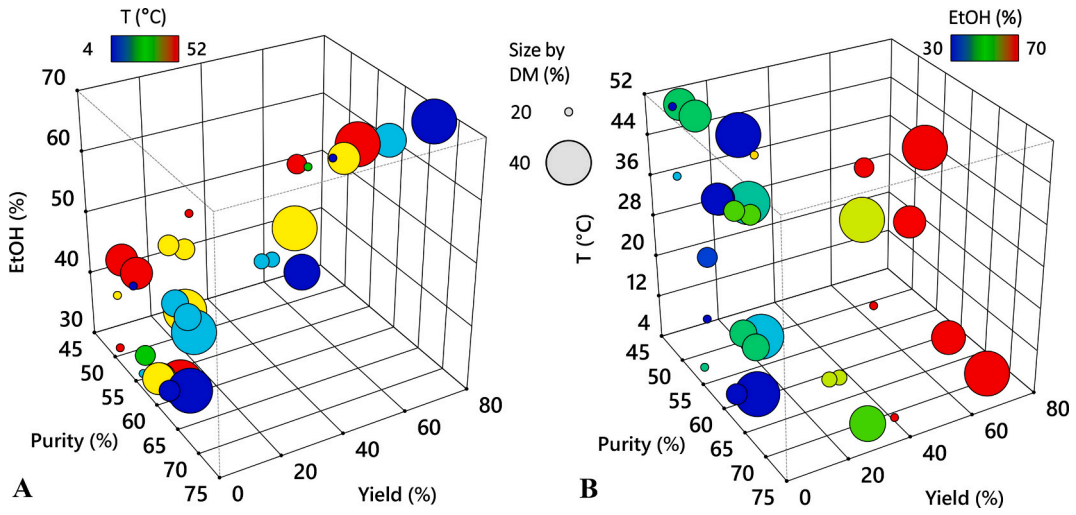

Fig. 6. Response values over input parameters. A) Precipitation yield (*Y*) in relation to the concentrate dry mass (w/w) and the precipitate purity (*P*) over applied ethanol fraction (*EtOH*). The varying temperature (*T*) is shown in color, the size of the circles correlates with the dry mass content (*DM*) of the samples during precipitation. B) Plot of the two response variables (*Y*, *P*) over the precipitation temperature (*T*). Here, the dry mass content (*DM*) of the samples correlates with the size of the circles and the ethanol content (*EtOH*) is shown in color.

% w/w) are necessary to achieve high $P \geq 60$ % and $Y \geq 35$ %. However, high *P* can also be attained with lower *EtOH* levels (≥ 40 % w/w) if the precipitation temperature (*T*) is not too high and the dry mass content (*DM*) is appropriately adjusted. In process design, the focus (i.e., greater weighting) should be on *Y*, as further separation of carbohydrates from the concentrate is only feasible through resource-intensive options, such as multi-stage precipitation involving significant process and energy effort (Peng et al., 2010; Vegas et al., 2005). Considering the constantly high *P* values (Fig. 6), a maximization of *Y* may be more effective for application in biorefineries. Especially for the applied simple autohydrolysis process approach, this can be expedient since the carbohydrates are *a priori* water-soluble and can be used in further purification and conversion steps (e.g., enzymatic or chemical) after precipitation. Therefore, if hemicellulose polysaccharides are to be separated after an autohydrolysis reaction, it is more effective in terms of auxiliary material consumption to separate them early in the process cascade and as completely as possible. The solid intermediate can then be used in concentrated form (with maximum solids loading) in an individual purification strategy for the applications, i.e., large and diluted streams no longer need to be processed.

The results of the multi-objective optimization in Fig. 5 highlight important relationships for potential applications within the investigated range. However, the dry mass content (*DM*) of the concentrate can be further increased with relatively little effort compared to further intensification via *EtOH* and *T*. For systematic investigation, the maximum *DM* value was set at 40 % (Table 1) based on preliminary tests showing that at higher *DM* levels spontaneous precipitation likely due to solution super saturation occurred without ethanol addition. Increasing the *DM* to 50 % or higher is technically feasible and might even offer significant synergies (Parsin et al., 2025). This adjustment could reduce the amount of solvent (here ethanol) used while achieving similar results for *Y* leading to further removal of impurities to enhance *P*. An increase in *DM* can be achieved, e.g., mechanically via membrane processes in combination with multi-effect evaporators; such options have already been investigated and modeled for the reference concept and show great potential for savings in the energy required in the hemicellulose-first concept (Parsin et al., 2025). Applying the derived relationships in section 3.3 and 3.4 and higher dry mass contents in biorefineries may therefore significantly reduce the energy requirements for precipitation (i.e., for cooling and ethanol recovery). However, a suitable operating point should be derived from energy and mass balances in order to take into account the trade-off between the additional efforts required to achieve a high dry mass content and the potential savings.

Fig. 5 indicates that for *DM* values above ca. 28 %, the impact on the two response variables *Y* and *P*, is opposite; both variables cannot be maximized simultaneously by altering *DM*. However, the response parameter *P* is considerably less pronounced to changes in *DM* or *T* (i.e., lower slope of the function) than the response parameter *Y*. Considering the normalized and quantified effects of the input variables in the coded range shown in Table 4, it becomes evident that the linear regression coefficients c_A show a monotonic influence on both response variables (*Y* and *P*). Therefore, a change in the input variable *DM* results in a larger absolute change of the *Y* function compared to the linear range of the *P* function (Table 4). This implies that using a concentrate with higher *DM* significantly increases *Y* without substantially reducing *P*. This difference can potentially be used to increase *Y* in the precipitation step, as further purification steps may be necessary anyway, depending on the application of the precipitate. The functions $Y = f(DM, EtOH, T)$ and $P = g(DM, EtOH, T)$ in Equations (9) and (10) provide a framework to estimate *Y* and *P* under comparable conditions. These relationships have so far proved robust and should apply again at higher *DM* once the super saturated conditions have been overcome.

To achieve high *Y* with simultaneous high *P* in carbohydrate precipitation following autohydrolysis of lignocellulose (such as wheat straw), as shown in Table 3, it is crucial to focus on raw material preparation and the autohydrolysis process itself. Both values can only be increased simultaneously if the hemicellulose hydrolysate already consists primarily of the target fraction (in this case, arabinoxylan; Table 2) and contains as few impurities as possible. The subsequent hydrolysate processing should aim to further reduce impurities with minimal effort and increase the proportion of the target fraction in the concentrate (Fig. 1). Key steps include the following.

- Removal of selected inorganic and organic components (e.g., dust, particles, proteins, secondary plant substances, phenolic components) during feedstock preparation.
- Optimization of autohydrolysis for the target fraction (i.e., maximizing the solubilization of arabinoxylan while minimizing solubilization of other biomass components).
- Removal of impurities produced during autohydrolysis and enrichment of the target fraction.

Considering the comparatively low specific energy demand of raw material preparation and mild saturated steam autohydrolysis, a combination with membrane processes for hydrolysate treatment can reduce impurities and simultaneously enrich the carbohydrates offering synergies for a subsequent precipitation (Parsin et al., 2025). Given the relatively high carbohydrate content of the precipitate (Table 3), even without significant purification steps, such a concept is promising in terms of providing water-soluble xylans for conversion into high-value products (e.g., pure xylooligosaccharides (Yegin, 2023), pentosan polysulfate (Alekseeva et al., 2020)). Including precipitation, the main disadvantages of an autohydrolysis concept in this context, namely contamination of xylans by inhibitors such as phenols, furfural and hydroxymethylfurfural, complex product purification, and noxious auxiliaries, can be avoided (Amorim et al., 2019).

5. Conclusion

This study aimed at intensifying xylan precipitation from hemicellulose derived via saturated steam autohydrolysis of wheat straw. Highly significant regression models demonstrated clear, mathematically describable relationships between process parameters and precipitation outcomes. A focused analysis of interactions among process parameters revealed substantial potential for process intensification. While high feed solution dry mass content and low precipitation temperatures contribute significantly, ethanol fraction exerts the most substantial influence on precipitation yield and precipitate purity. Notably, without further purification, the carbohydrate content of the precipitated wheat straw xylan approaches the purity levels of commercial laboratory xylan standards. Nevertheless, the precipitate differs in composition, exhibiting, for instance, a markedly elevated glucose content. An optimized hemicellulose-first process design enables achieving these high carbohydrate contents in the precipitate along with very high yields. These findings indicate that while increased dry mass content effectively drives yield, an optimized balance with ethanol fraction and precipitation temperature provides a viable strategy for process integration in biorefineries. Future research should assess the applicability of these derived correlations to other crop residues.

Using wheat straw xylan as an example, this study illustrates how systematic optimization elucidates precipitation correlations, thereby enhancing efficiency while reducing raw material demand and process effort. These results are currently constrained to the experimental conditions investigated. Confirmation of these outcomes in continuous and integrated process concepts could significantly advance overcoming key hurdles to the economic viability of next-generation biorefineries. Despite inherent challenges in scaling laboratory findings to industrial applications, this study advances fundamental understanding of carbohydrate precipitation and provides a robust framework for its application in biorefineries.

Declaration of Generative AI and AI-assisted technologies in the writing process

During the preparation of this work the authors used DeepL (DeepL, Köln, Germany) in order to improve the readability and language of the manuscript. After using, the authors reviewed and edited the content as needed and take full responsibility for the content of the published article.

CRediT authorship contribution statement

Stanislav Parsin: Writing – review & editing, Writing – original draft, Visualization, Validation, Resources, Methodology, Investigation, Funding acquisition, Formal analysis, Data curation, Conceptualization. **Martin Kaltschmitt:** Writing – review & editing, Supervision, Project administration, Funding acquisition.

Declaration of competing interest

The authors declare that they have no known competing financial interests or personal relationships that could have appeared to influence the work reported in this paper.

Acknowledgements

This work was supported by the German Federal Ministry of Education and Research (grant number: 031B0660F) and the BWFGB (Behörde für Wissenschaft, Forschung, Gleichstellung und Bezirke der Freien und Hansestadt Hamburg) (grant number: C4T718).

Appendix A. Supplementary data

Supplementary data to this article can be found online at https://doi.org/10.1016/j.biortech.2026.134963.

Data availability

Data will be made available on request.

References

Alekseeva, A., Raman, R., Eisele, G., Clark, T., Fisher, A., Lee, S.L., Jiang, X., Torri, G., Sasisekharan, R., Bertini, S., 2020. In-depth structural characterization of pentosan polysulfate sodium complex drug using orthogonal analytical tools. Carbohydr. Polym. 234, 115913. https://doi.org/10.1016/j.carbpol.2020.115913.

Amorim, C., Silvério, S.C., Prather, K.L.J., Rodrigues, L.R., 2019. From lignocellulosic residues to market: production and commercial potential of xylooligosaccharides. Biotechnol. Adv. 37, 107397. https://doi.org/10.1016/j.biotechadv.2019.05.003.

Brownell, H.H., Saddler, J.N., 1987. Steam pretreatment of lignocellulosic material for enhanced enzymatic hydrolysis. Biotechnol. Bioeng. 29, 228–235. https://doi.org/10.1002/bit.260290213.

Chen, Z., Świsłocka, R., Choińska, R., Marszałek, K., Dąbrowska, A., Lewandowski, W., Lewandowska, H., 2024. Exploring the Correlation between the Molecular Structure and Biological Activities of Metal-Phenolic compound Complexes: Research and Description of the Role of Metal Ions in improving the Antioxidant Activities of Phenolic Compounds. Int. J. Mol. Sci. 25, 11775. https://doi.org/10.3390/ijms252111775.

Cheng, J., Chen, T., Liu, X., Zhou, X., Zhan, Y., Huang, C., Fang, G., Huang, C., 2024. A lignin-first biorefinery by integrated deep eutectic solvents towards formaldehyde-free plywood adhesive and monomeric sugars. Chem. Eng. J. 499, 155980. https://doi.org/10.1016/j.cej.2024.155980.

Goos, P., Jones, B., Syafitri, U., 2016. I-Optimal Design of Mixture Experiments. J. Am. Stat. Assoc. 111, 899–911. https://doi.org/10.1080/01621459.2015.1136632.

Han, Q.-B., 2018. Critical Problems Stalling Progress in Natural Bioactive Polysaccharide Research and Development. J. Agric. Food Chem. 66, 4581–4583. https://doi.org/10.1021/acs.jafc.8b00493.

Harman, R., Filová, L., Richtárik, P., 2020. A Randomized Exchange Algorithm for Computing Optimal Approximate designs of Experiments. J. Am. Stat. Assoc. 115, 348–361. https://doi.org/10.1080/01621459.2018.1546588.

Hu, X., Goff, H.D., 2018. Fractionation of polysaccharides by gradient non-solvent precipitation: a review. Trends Food Sci. Technol. 81, 108–115. https://doi.org/10.1016/j.tifs.2018.09.011.

Jacquemin, L., Zeitoun, R., Sablayrolles, C., Pontalier, P.-Y., Rigal, L., 2012. Evaluation of the technical and environmental performances of extraction and purification processes of arabinoxylans from wheat straw and bran. Process Biochem. 47, 373–380. https://doi.org/10.1016/j.procbio.2011.10.025.

Kishani, S., Escalante, A., Toriz, G., Vilaplana, F., Gatenholm, P., Hansson, P., Wagberg, L., 2019. Experimental and Theoretical Evaluation of the Solubility/Insolubility of Spruce Xylan (Arabino Glucuronoxylan). Biomacromolecules 20, 1263–1270. https://doi.org/10.1021/acs.biomac.8b01686.

Lai, B., Plan, M., Hodson, M., Krömer, J., 2016. Simultaneous Determination of Sugars, Carboxylates, Alcohols and Aldehydes from Fermentations by High Performance Liquid Chromatography. Fermentation 2, 6. https://doi.org/10.3390/fermentation2010006.

Lin, Q., Zhan, Q., Wu, Y., Wang, J., Li, L., Peng, F., Xu, F., Ren, J., 2023. Molecular scale behavior of xylan during solvent-controlled extraction and precipitation. PCCP 25, 28078–28085. https://doi.org/10.1039/D3CP01385E.

Liu, H., Zhu, J.Y., Fu, S.Y., 2010. Effects of lignin-metal complexation on enzymatic hydrolysis of cellulose. J. Agric. Food Chem. 58, 7233–7238. https://doi.org/10.1021/jf1001588.

Lynd, L.R., Beckham, G.T., Guss, A.M., Jayakody, L.N., Karp, E.M., Maranas, C., McCormick, R.L., Amador-Noguez, D., Bomble, Y.J., Davison, B.H., Foster, C., Himmel, M.E., Holwerda, E.K., Laser, M.S., Ng, C.Y., Olson, D.G., Román-Leshkov, Y., Trinh, C.T., Tuskan, G.A., Upadhayay, V., Vardon, D.R., Wang, L., Wyman, C.E., 2022. Toward low-cost biological and hybrid biological/catalytic

conversion of cellulosic biomass to fuels. Energ. Environ. Sci. 15, 938–990. https://doi.org/10.1039/D1EE02540F.
Mujtaba, M., Fernandes Fraceto, L., Fazeli, M., Mukherjee, S., Savassa, S.M., Araujo de Medeiros, G., do Espírito Santo Pereira, A., Mancini, S.D., Lipponen, J., Vilaplana, F., 2023. Lignocellulosic biomass from agricultural waste to the circular economy: a review with focus on biofuels, biocomposites and bioplastics. J. Clean. Prod. 402, 136815. https://doi.org/10.1016/j.jclepro.2023.136815.
Naidu, D.S., Hlangothi, S.P., John, M.J., 2018. Bio-based products from xylan: a review. Carbohydr. Polym. 179, 28–41. https://doi.org/10.1016/j.carbpol.2017.09.064.
Overend, R.P., Chornet, E., 1987. Fractionation of lignocellulosics by steam-aqueous pretreatments. Philosophical transactions of the Royal Society of London. Series a, Mathematical and Physical Sciences 321, 523–536. https://doi.org/10.1098/rsta.1987.0029.
Parsin, S., Kaltschmitt, M., 2023. Processing of hemicellulose in wheat straw by steaming and ultrafiltration - a novel approach. Bioresour. Technol. 393, 130071. https://doi.org/10.1016/j.biortech.2023.130071.
Parsin, S., Kaltschmitt, M., 2025. Intensification of wheat straw autohydrolysis at minimal water input: advancing a novel hemicellulose-first approach. Green Chem. 27, 8532–8548. https://doi.org/10.1039/D5GC02300A.
Parsin, S., Scherzinger, M., Kaltschmitt, M., 2025. Energy-Related Assessment of a Hemicellulose-first Concept—Debottlenecking of a Hydrothermal Wheat Straw Biorefinery. Molecules 30, 602. https://doi.org/10.3390/molecules30030602.
Peng, F., Ren, J.-L., Xu, F., Bian, J., Peng, P., Sun, R.-C., 2009. Comparative Study of Hemicelluloses Obtained by Graded Ethanol Precipitation from Sugarcane Bagasse. J. Agric. Food Chem. 57, 6305–6317. https://doi.org/10.1021/jf900986b.
Peng, F., Ren, J.-L., Xu, F., Bian, J., Peng, P., Sun, R.-C., 2010. Fractional study of alkali-soluble hemicelluloses obtained by graded ethanol precipitation from sugar cane bagasse. J. Agric. Food Chem. 58, 1768–1776. https://doi.org/10.1021/jf9033255.
Pronyk, C., Mazza, G., 2012. Fractionation of triticale, wheat, barley, oats, canola, and mustard straws for the production of carbohydrates and lignins. Bioresour. Technol. 106, 117–124. https://doi.org/10.1016/j.biortech.2011.11.071.
Qaseem, M.F., Shaheen, H., Wu, A.-M., 2021. Cell wall hemicellulose for sustainable industrial utilization. Renew. Sustain. Energy Rev. 144, 110996. https://doi.org/10.1016/j.rser.2021.110996.
Rao, J., Lv, Z., Chen, G., Peng, F., 2023. Hemicellulose: Structure, chemical modification, and application. Prog. Polym. Sci. 140, 101675. https://doi.org/10.1016/j.progpolymsci.2023.101675.
Renders, T., van den Bosch, S., Koelewijn, S.-F., Schutyser, W., Sels, B.F., 2017. Lignin-first biomass fractionation: the advent of active stabilisation strategies. Energ. Environ. Sci. 10, 1551–1557. https://doi.org/10.1039/C7EE01298E.
Safronov, A.P., Adamova, L.V., Kurlyandskaya, G.V., 2019. Flory–Huggins Parameters of Guar Gum, Xanthan Gum, Agarose, and Gellan Gum in Aqueous Solutions. Polym. Sci., Ser. A 61, 29–38. https://doi.org/10.1134/S0965545X19010139.
Santibáñez, L., Henríquez, C., Corro-Tejeda, R., Bernal, S., Armijo, B., Salazar, O., 2021. Xylooligosaccharides from lignocellulosic biomass: a comprehensive review. Carbohydr. Polym. 251, 117118. https://doi.org/10.1016/j.carbpol.2020.117118.
Scapini, T., Dos Santos, M.S.N., Bonatto, C., Wancura, J.H.C., Mulinari, J., Camargo, A.F., Klanovicz, N., Zabot, G.L., Tres, M.V., Fongaro, G., Treichel, H., 2021. Hydrothermal pretreatment of lignocellulosic biomass for hemicellulose recovery. Bioresour. Technol. 342, 126033. https://doi.org/10.1016/j.biortech.2021.126033.
Siebertz, K., van Bebber, D., Hochkirchen, T., 2010. Statistische Versuchsplanung: Design of Experiments (DoE). Springer, Berlin Heidelberg, Berlin, Heidelberg.
Singh, N., Singhania, R.R., Nigam, P.S., Dong, C.-D., Patel, A.K., Puri, M., 2022. Global status of lignocellulosic biorefinery: challenges and perspectives. Bioresour. Technol. 344, 126415. https://doi.org/10.1016/j.biortech.2021.126415.
Sluiter, A., B. Hames, R. Ruiz, C. Scarlata, J. Sluiter, D. Templeton, and D. Crocker: NREL, 2011. Determination of Structural Carbohydrates and Lignin in Biomass: Laboratory Analytical Procedure (LAP); Issue Date: April 2008; Revision Date: July 2011 (Version 07-08-2011).
Sluiter, A., R. Ruiz, C. Scarlata, J. Sluiter, and D. Templeton: NREL, 2008. Determination of Extractives in Biomass: Laboratory Analytical Procedure (LAP); Issue Date 7/17/2005.
Sun, D., Lv, Z.-W., Rao, J., Tian, R., Sun, S.-N., Peng, F., 2022. Effects of hydrothermal pretreatment on the dissolution and structural evolution of hemicelluloses and lignin: a review. Carbohydr. Polym. 281, 119050. https://doi.org/10.1016/j.carbpol.2021.119050.
Swennen, K., Courtin, C.M., van der Bruggen, B., Vandecasteele, C., Delcour, J.A., 2005. Ultrafiltration and ethanol precipitation for isolation of arabinoxylooligosaccharides with different structures. Carbohydr. Polym. 62, 283–292. https://doi.org/10.1016/j.carbpol.2005.08.001.
Tang, W., Liu, D., Yin, J.-Y., Nie, S.-P., 2020. Consecutive and progressive purification of food-derived natural polysaccharide: based on material, extraction process and crude polysaccharide. Trends Food Sci. Technol. 99, 76–87. https://doi.org/10.1016/j.tifs.2020.02.015.
Thanh, N.T.K., Maclean, N., Mahiddine, S., 2014. Mechanisms of nucleation and growth of nanoparticles in solution. Chem. Rev. 114, 7610–7630. https://doi.org/10.1021/cr400544s.
van Delft, F., van Langeveld, A.D., Nieuwenhuys, B.E., 1985. Determination of nucleation and growth mechanisms. Thin Solid Films 123, 333–351. https://doi.org/10.1016/0040-6090(85)90008-2.
Vegas, R., Alonso, J.L., Domínguez, H., Parajó, J.C., 2004. Processing of rice husk autohydrolysis liquors for obtaining food ingredients. J. Agric. Food Chem. 52, 7311–7317. https://doi.org/10.1021/jf049142t.
Vegas, R., Alonso, J.L., Dominguez, H., Parajo, C.Juan, 2005. Manufacture and refining of Oligosaccharides from Industrial Solid Wastes. Ind. Eng. Chem. Res. 44, 614–620. https://doi.org/10.1021/ie049289.
Xu, J., Yue, R.-Q., Liu, J., Ho, H.-M., Yi, T., Chen, H.-B., Han, Q.-B., 2014. Structural diversity requires individual optimization of ethanol concentration in polysaccharide precipitation. Int. J. Biol. Macromol. 67, 205–209. https://doi.org/10.1016/j.ijbiomac.2014.03.036.
Yegin, S., 2023. Microbial xylanases in xylooligosaccharide production from lignocellulosic feedstocks. Biomass Convers. Biorefin. 13, 3619–3658. https://doi.org/10.1007/s13399-022-03190-w.
Zabed, H., Sahu, J.N., Boyce, A.N., Faruq, G., 2016. Fuel ethanol production from lignocellulosic biomass: an overview on feedstocks and technological approaches. Renew. Sustain. Energy Rev. 66, 751–774. https://doi.org/10.1016/j.rser.2016.08.038.
Zasadowski, D., Yang, J., Edlund, H., Norgren, M., 2014. Antisolvent precipitation of water-soluble hemicelluloses from TMP process water. Carbohydr. Polym. 113, 411–419. https://doi.org/10.1016/j.carbpol.2014.07.033.
Zhou, Z., Liu, D., Zhao, X., 2021. Conversion of lignocellulose to biofuels and chemicals via sugar platform: an updated review on chemistry and mechanisms of acid hydrolysis of lignocellulose. Renew. Sustain. Energy Rev. 146, 111169. https://doi.org/10.1016/j.rser.2021.111169.